

RELATIONSHIP BETWEEN LULC CHARACTERISTIC AND LST USING REMOTE SENSING AND GIS, CASE STUDY GUELMA (ALGERIA)

IMEN GUECHI*, HALIMA GHERRAZ**, DJAMEL ALKAMA***

Key-words: Guelma city; urbanization; landscape; Multi-Buffer Ring; LST; remote sensing & GIS.

Abstract. Urbanization is a phenomenon that is driven by humans. It has significantly influenced biodiversity, ecosystem processes and regional climate. Like all medium-sized cities in Algeria, Guelma is affected by the rapid and massive urban growth which has increased the land use/land cover (LULC) changes. Thus, it generates climate change. This work explores the relationship between the LULC characteristic and LST, based on remote sensing & GIS. A time-series of Landsat images TM, ETM+ and OLI/TIRS data and various geospatial approaches as well as the urban – rural gradient, multi-buffer ring, statistics and the techniques used in urban landscape metrics were used in order to facilitate the analysis. The findings have revealed that urban/built-up areas of Guelma city have increased by 12%. However, the agricultural and forest areas have witnessed a reduction of 15% and 3%. The average temperature of the urban setting was 38.27 C° in 1986, whereas in 2019 it reached 41.90 C°. When the average temperature values for every class were calculated, it was observed that the lowest values were in forest bodies with 27.26 C° in 1986 and 37.78 C° in 2019. There is a possible rise in LST over time scale owing to the substitution of green cover by urban soil areas. For instance, there was a noticeable increase of 3.65°C in mean LST for urban areas. The increased urban LST values are due to the broad region, the low fragmentation degree of landscape and complex outlines, which in turn lead to reduced forest LST values. In comparison to the LST of the sprawl form, the LST of compact form is low. This investigation provides us with clear understanding of the impact that the urbanization, composition and form of landscape has on LST. These findings have significant theoretical and managerial implications.

1. INTRODUCTION

Urbanization is one of the most important factors triggering a transition in (LULC) (Pal *et al.*, 2017). It is an urban phenomenon that has drawn the attention of researchers in the 21st century (Spence *et al.*, 2009). Urban areas such as cities and towns comprise more than half of the world's population. This number is expected to rise to about five billion by 2030. UNFPA also predicts that much of this urbanization that would occur in Africa and Asia would bring enormous social, economic and environmental problems (UNFPA, 2017). Change in land use/land cover (LULC) has a major impact on climate through various pathways. Those pathways are found to modulate the surface energy balance which affects the land surface temperature (LST). This leads to changes in the region's micro-climate (Wang *et al.*, 2018; Gogoi *et al.*, 2019; Jain *et al.*, 2017). This local temperature variation has a negative effect on both people and the environment because it hinders air quality, increases energy consumption, affects biological control and human health (Meineke *et al.*, 2014; Plocoste *et al.*, 2014). LST is considered a significant urban climate indicator in which the temperature in urban environments and the increasing areas of built-up surfaces is higher than in areas covered by vegetation and water. Therefore, studying the impact of urbanization on LST is important because it can disrupt a wide variety of natural processes (Carleton *et al.*, 2016; Tan *et al.*, 2020). In addition, the surface climate

* Ph.D., Department of Architecture, Laboratory of Evaluation of Quality in Architecture and In-built Environment, University of Arbi Ben M'hidi, Oum El Bouaghe, Algeria, guechi.imen@gmail.com.

** Ph.D., Department of Architecture, Laboratory of Evaluation of Quality in Architecture and In-built Environment, University of Arbi Ben M'hidi, Oum El Bouaghe, Algeria, halima.gherraz@gmail.com.

*** Professor, Department of Architecture, University of Guelma, Algeria, dj.alkama@gmail.com.

can be affected by changes in urban space and by the removal of vegetation due to urbanization (Das *et al.*, 2020).

Compared to conventional observation methods which are used at meteorological stations, remote sense tracking of LST provides a wide range of measurements and good spatial consistency. This technique has therefore grown rapidly in thermal environmental research (Liu *et al.*, 2016; Wang *et al.*, 2018). The use of remote sensing data in conjunction with Geographic Information Systems (GIS) is effective in mapping urban areas, modelling urban growth, monitoring LULC's dynamic changes and estimating LST (Kimuku *et al.*, 2017). By incorporating thermal remote sensing, LST information is available from a series of satellite sensors (such as Landsat, MODIS, and ASTER) which cover an extensive part of the earth's surface. At different temporal scales, thermal imaging generates full spatial coverage in comparison to the air temperatures from the weather stations (Myint *et al.*, 2013). Therefore, the relationship between LST and (LULC) change should be investigated in order to address further regional environmental issues and provide a basis for regional planning (Pal *et al.*, 2017). For the effective use and management of natural resources, it is very important to quantify the causes and consequences of LULC shift. (Li *et al.*, 2018).

Several items of research have been published to study: first the relationship between LST / LULC (an increase in land surface temperatures (LST) is one of the main effects of LULC changes) especially in urban centres (Aboelnour and Engel, 2018; Pal and Ziaul, 2017). Second, the relationship between LST and the Landscape patterns which are based on the use of different LST inverting methods has been studied (Brown *et al.*, 2016). The study has also shown that underlying landscape trends have an important impact on LST (Peng *et al.*, 2016; Estoque *et al.*, 2017). Third, the relation between urban form and climate was explored by spatial distribution and the use of morphological indices (Martinelli *et al.*, 2017). There are various approaches and techniques for analysing urban form indices, including the use of spatial metrics (Yang *et al.*, 2016; Boogaard *et al.*, 2017; Santos *et al.*, 2017). They are also commonly used to assess the effects of landscape trends on surface landscape temperature (LST) (Asgarian *et al.*, 2015; Chen and Yu, 2017). Fourth, the relationships between LST, Normalized Difference built-up Index (NDBI), and Normalized Difference Vegetation Index (NDVI) were established using Linear Regression (Guha *et al.*, 2018; Ferrelli *et al.*, 2018). The present study will provide an in-depth analysis of the relation between the LULC characteristic (Urban density, urban form, Landscape pattern and land cover types) and LST by the integration of a geographical and economic approach in the same case study to determine the main effects of landscape characteristic on LST.

Guelma is affected by rapid and massive urban growth which has strongly disrupted the space. This urban growth generates profound spatial and environmental transformations (Guechi *et al.*, 2017). The local authorities of Guelma have revised the Master Plan for Development and Urban Planning (PDAU) in 2013 so as to provide solution for land availability for the future urbanization of Guelma municipality. They have recourse to the inter-communal group of Guelma as part of the postponement of urban growth from the municipality of Guelma to neighbouring municipalities. It included the chief city of Guelma, and the three neighbouring communes including El Fdjouj, Belkhair and Ben Djarah. The position of Guelma in the centre places these communes in its field of attraction. It suffers from the burden of the communes of the wilaya in general and the neighbouring communes in particular. Due to their proximity to the large urban centre and containing land with high agricultural potential, the towns of Belkheir, El Fedjoudj and Bendjerrah have not experienced the desired growth. This raises the potential to exploit agricultural land and forests for urban purposes. Reducing vegetation and replacing it with impermeable surfaces, such as asphalt and concrete, is directly related to urbanization factors that have environmental and social consequences (Mitchell, 2011).

This research objective is to determine and analyse the relationship between LULC characteristics and land surface temperature (LST) in the context of urbanization from 1986 to 2019 in Guelma, using remote sensing & GIS. In order to investigate the urban expansion in Guelma, the time-series satellite images with supervised technique for classification of Maximum Likelihood (MLC) is

employed. Also, in order to determine and analyse the connection between LST and main LULC characteristics (Urban density, urban form, Landscape pattern and land cover types), a multi-buffer ring method, quantitative Study of LST and Landscape metrics technique of land cover are applied.

2. STUDY AREA

Our case study (Guelma inter-municipal grouping) is situated in the centre of Guelma province, northeast Algeria. It is approximately “60 km” south of the Mediterranean Sea $36^{\circ}27'43''N - 7^{\circ}25'33''E$ and 305 m above sea level (Fig. 1). This region occupies a total area of 282.11 km². It has a semi-arid climate with cool winters. It has an average annual temperature of 21.5 °C and 150.3 mm average of annual rainfall (Aouissi, 2010.). It is possible to distinguish two periods in the year, eight months of cold and wet weather from October to May and four months of hot and dry weather from June to September. It is a group of four municipalities (the chief town of the Wilaya, the municipality of Bendjarah, the municipality of Belkheir and the municipality of el Fdjouj). They are in a context of an agricultural vocation par excellence. The position of Guelma in the centre places these municipalities in its field of attraction.

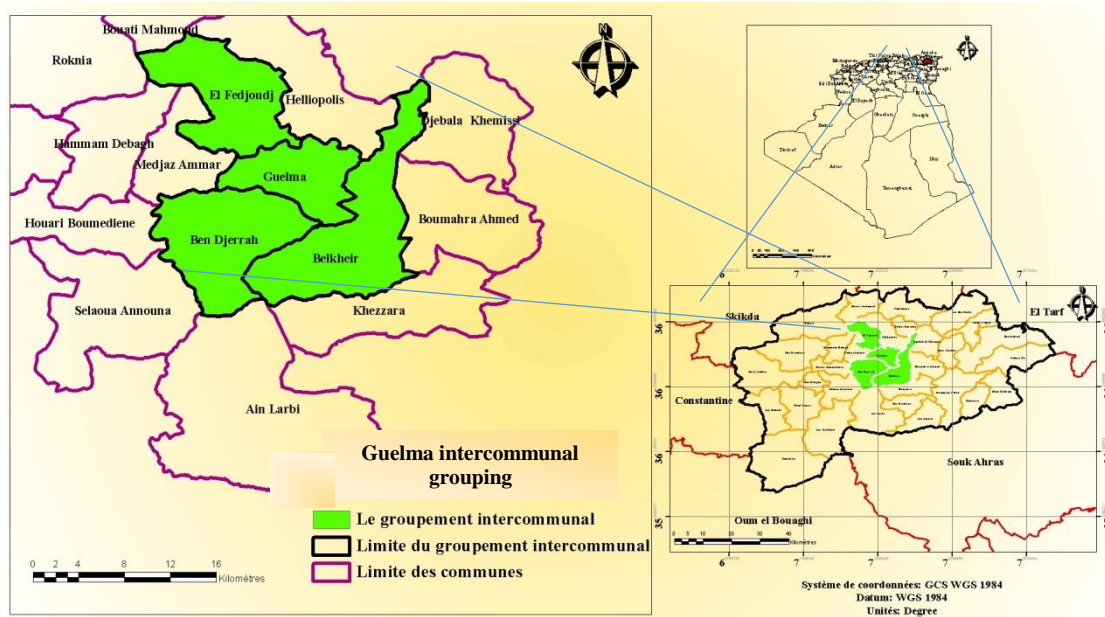


Fig. 1 – Location map of Guelma inter-communal grouping.

3. METHDOLOGY

3.1. Image acquisition and pre-processing

The main data sets in this analysis were time series of Landsat images which were captured by Landsat TM, Landsat ETM+, and Landsat Operational Land Imager (OLI)/Thermal Infrared Sensor (TIRS) sensors. The data are presented in Table 1. The selected satellite data was cloud-free. All datasets have been downloaded as a georeferenced data set from the website of the United States Geological Survey (USGS) (<https://earthexplorer.usgs.gov>). Satellite images were acquired at an interval of 4–5 years during the same season (the dry season) in order to prevent phenological

variability. The Image processing software ArcGIS Spatial Analyst (version 10.5), Environment for Visualizing Images (ENVI) version 5.0, Fragstat 4.2 and Excel were used for conducting the statistical analysis.

Table 1

Landsat data specification used in the study

LANDSAT_SCENE_ID	SPACECRAFT_ID	Acquisition Date	UTM_ZONE	Spatial Resolution
LT51930351986180FUI00	L5_TM	29/06/1986	32	30
LT51930351990159FUI00	L5_TM	08/06/1990	32	30
LT51930351996160FUI00	L5_TM	08/06/1996	32	30
LE71930352000179FUI00	L7_ETM	27/06/2000	32	30
LE71930352005176EDC00	L7_ETM	25/06/2005	32	30
LE71930352010174EDC00	L7_ETM	23/06/2010	32	30
LC81930352015180LGN01	LANDSAT_8	29/06/2015	32	30
LC81930352019159LGN00	LANDSAT_8	19/06/2019	32	30

In this research, after using a radiometric calibration, the fast line-of-sight atmospheric analysis of hypercube (FLAASH) was used for atmospheric correction in ENVI5.1 software. Some parameters are considered for running FLAASH including satellite overpass time, sensor altitude, geographical location, region-related specific atmospheric model, and solar zenith angle of the satellite images acquired by Landsat 5, 7, and 8. The Flowchart Fig. 2 shows the methodology adopted for the following study.

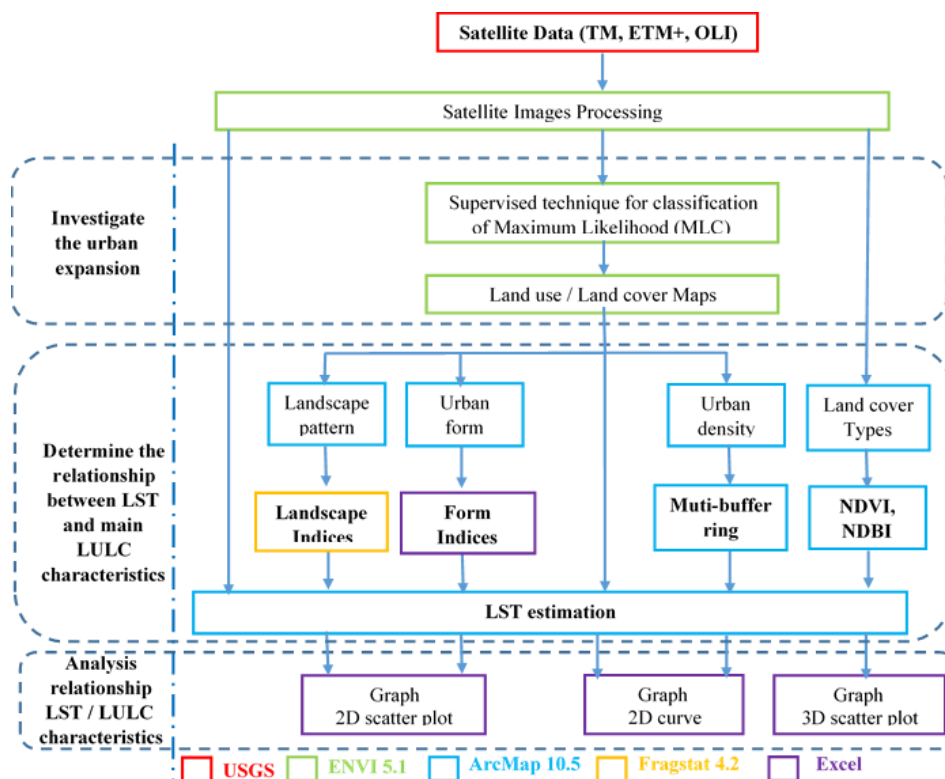


Fig. 2 – Flow chart explaining the methodology.

3.2. Classification of satellite images

Remotely sensed data are commonly used for mapping land use and cover maps. Supervised technique for classification of Maximum Likelihood (MLC) is employed in this study. MLC which is used in a variety of applications is the most generally used supervised classification (Pushpendra *et al.*, 2014). MLC doesn't only perform better than the other parametric classifications but it also considers the variance-covariance within the class distributions (Erdas, 1999). Images from the years 1986, 1990, 1996, 2000, 2005, 2010, 2015 and 2019 were classified with the software ENVI 5.1 so as to obtain land cover distribution. Composite imagery with false colour band combination of bands RGB = 543 for Landsat 8, RGB = 432 for Landsat 5TM and Landsat 7 ETM+ was utilized to obtain better visualization of the urban environments. Four signature classes were selected for the classification including urban, forest, agricultural and bare land. Residential buildings, highways, industries, commercial buildings illustrate the urban area. The bare land represents the soil and unused land. The agricultural land represents both the areas with and without vegetation. Training areas have been developed by selecting one or more polygons for each class. Pixels were taken to be the training pixels for a specific class within the training area. Then, Confusion Matrix Using Ground Truth ROIs in ENVI5.0 was used in this analysis to test the accuracy of maximum likelihood classification. The Kappa coefficient was also obtained for each year.

3.3. LULC characteristics

3.3.1. Urban density

From a socio-economic point of view, cities are perceived as magnets that provide people with different social and economic opportunities. Cities can draw or repel residents, money, as well as business investment (Fonseka *et al.*, 2019.). This feature of the city is well illustrated by the multi-buffer approach which demonstrates the city's distribution outward from its centre (Fonseka *et al.*, 2019; Rahman, 2016). The position of Guelma in the centre, places these municipalities in its attraction sector. Taking into consideration the idea of magnetic cities, the multi-buffer ring method was employed. From 1 km to 16 km, the multi-buffer rings are created in Arc GIS (using the multiple ring buffer option) for every 1km distance from Guelma centre to outside. Then, the classified intersection with land cover for all dates is carried out. Later on, the urban area class is calculated for a distance of 16 km. The density is extracted by the equation that follows:

$$\text{Urban density} = (\text{Urban area per ring}) / (\text{Total area of ring}) \dots \dots \dots (1)$$

3.3.2. Urban form Indices

In this study, we opted to use the most elementary arithmetic indices (Guérois, 2003). To measure the urban form of the inter-municipal Grouping of Guelma, several form indices were set up based on the different geometric relationships between the following elementary values including the perimeter, the surface area and the axes digitation distances (Table 2).

Table 2

Urban form Indices

Urban forme indices	Objectif	Formuler
I1 (Perimetercontortion index)	describe the degree of irregularity of the contour shape	$I_1 = 4\pi A/P^2$
I2 (The Stretch Index)	measures the stretch, or span of the shape	$I_2 = L2/L1$
I3, I4, I5 (Disc filling indices)	measure disc filling of the shape	$I_3 = \pi(R_{ci})^2/A, I_4 = R_{ci}/R_{cc}, I_5 = A/\pi(R_{cc})^2$
I6 (The digitation index)	identify more clearly the digested forms	$I_6 = 1/(1 +D)$

P: perimeter, **A**: shape area, **L2**: the length of longest axis, **L1**: the length of longest perpendicular axis, **R_{ci}**: radius of the largest circle, **R_{cc}**: radius of the smallest circumscribed circle.

3.3.3. Landscape Pattern Indices

Indices were chosen from patch type and landscape level to quantitatively describe the characteristics of LC's landscape patterns. Landscape level indices are used to define the overall LC status characteristics, whereas, patch type indices concentrate on LCT types morphology and structure. The selected landscape indices including total area (CA), percent landscape (PLAN), largest patch index (LPI), mean patch area (AREA_MN), landscape shape index (LSI), Euclidean nearest neighbour distance (ENN). These are typical and frequently utilized hints in landscape research.

In order to quantitatively investigate the correlation between the landscape pattern indices, the LST and the underlying surface coverage area, ArcGIS ' fishing net feature was used to extract 15 * 17 samples with a 1400 m 1400 m grid unit. The sampled fields were then superimposed with the vector map LC and LST. After that they were converted to a grid file. In order to estimate the indices for the landscape pattern, the grid data were input into Frag stats 4.2.

3.3.4. Land Cover Types

- The **NDVI** index is a measure of the surface vegetation quantity and vigour. For the reason that vegetation is well reflected in the near infrared part of the spectrum, NDVI has become a simple graphic indicator for assessing target vegetation coverage. Several researches focused on understanding the LST-NDVI relationship (Lo *et al.*, 1997). The NDVI images were calculated with the equation (2). $NDVI = (NIR - Red) / (NIR + Red)$ (2) where Red and NIR are the spectral reflectance of vegetation, NIR : is the near infrared band, Red: is the red band
- **NDBI** is another index used in this study that is sensitive to the built-up area. It is derived by the following equation: $NDBI = (R_{SWIR} - R_{NIR}) / (R_{SWIR} + R_{NIR})$ (3)
Where, R_{SWIR} and R_{NIR} are the spectral reflectance.

3.4. LST Estimation

The thermal infrared bands of different Landsat image types (band 6 of Landsat 5 TM, Landsat 7 ETM+ and band 10 of Landsat 8) (Landsat (7), 2011; Landsat (8), 2015) were utilized to estimate LST of the inter-municipal grouping of Guelma. Landsat OLI-TIRS had two thermal bands which are band 10 and band 11. Since band 11 displays striping, only band 10 was used here. A single window algorithm based on NDVI was utilized to extract land surface emissivity (LSE). The steps below are employed to retrieve LST from thermal images and NDVI images.

a – Radiance image calculation

The raw digital number (DN) values of TM and ETM+ have been converted to luminance radiation or top-of-atmospheric (TOA) radiance by means of equation (1) (Chander *et al.*, 2003).

$$L\lambda = (L_{max} - L_{min}) / (QCAL_{max} - QCAL_{min}) \times (DN - QCAL_{min}) + L_{min} \dots\dots(4)$$

where,

DN : is the pixel digital number for band 6, $L_{max} = 17, 04$ (mW/cm²sr·m) is spectral at-sensor radiance that is scaled to $QCAL_{max}$, $L_{min} = 0$ (mW/cm²sr·m) is spectral at-sensor radiance that is scaled to $QCAL_{min}$, $QCAL_{max} = 255$ is Maximum quantized calibrated pixel value corresponding to L_{max} , $QCAL_{min} = 0$ is the minimum quantized calibrated pixel value corresponding to L_{min} .

For Landsat OLI-TIRS the equation (5) is used (USGS, 2014). $L\lambda = M_L \times DN + A_L$ (5)
where, M_L : is the specific multiplicative rescaling factor band DN : is the pixel digital number for band 10

A_L : is the specific additive rescaling factor band from the metadata.

b – Radiant temperature calculation

The following equation (6) was used to calculate radiant temperature by the use of radiance images which were obtained from thermal bands (Chander *et al.*, 2009). $T_k = K2/ln(K1/L\lambda + 1)$
 (6) Where, T_k : is the temperature in Kelvin (K), $K1$: is the prelaunch calibration of constant 1 in unit of $W/(m^2sr \cdot \mu m)$, $K2$: is the prelaunch calibration constant 2 in Kelvin.

c – Emissivity calculation:

The emissivity is calculated with the following equation $\varepsilon = 0.004 p_v + 0.986$ (7) Where, p_v : is the vegetation proportion which can be derived from the NDVI image based on the following equation (6). $P_v = \left(\frac{NDVI - NDVI_{min}}{NDVI_{max} - NDVI_{min}} \right)^2$ (8)

d – LST Calculation

Outputs derived from (5) and (7) were then used as inputs to estimate the LST using the equation below. $LST = T_k / (1 + ((\lambda T_k) / p) \ln \varepsilon)$(9) Where, λ : is the central wavelength (in μm) of the Landsat thermal band, $p = 1.438 \times 10^{-2} mK$.

3.5. The Relationship between LULC characteristics and LST

This study's main consideration was to define the relation between LST/LULC characteristics. In order to determine and analyse the mean LST values for land cover change and land use, class zonal statistics in ArcGIS were used. The relation between LST /LULC characteristics was statistically analysed in Excel software by means of regression analysis and trend analysis.

4. RESULTS

4.1. Precision evaluation report of LU / LC classification

The urban land cover classification results in the inter-municipal grouping of Guelma from 1986 to 2019 are shown in Fig. 3.

4.2. Spatio-temporal Pattern of LU/LC Dynamics and its Relationship with LST

The spatial LU/LC maps of inter-municipal grouping of Guelma are shown in Fig. 3. It is clear that there has been an urban expansion in the inter-municipal grouping of Guelma in the last 33 years. This growth is concentrated in the Guelma municipality which is very significant compared to the other municipalities. Guelma is regarded as one of the Algerian cities which fulfils very important urban functions. Those functions exert an influence on both the adjacent communes and even on the rest of the communes of the province, as indicated in the (PDAU 2013).

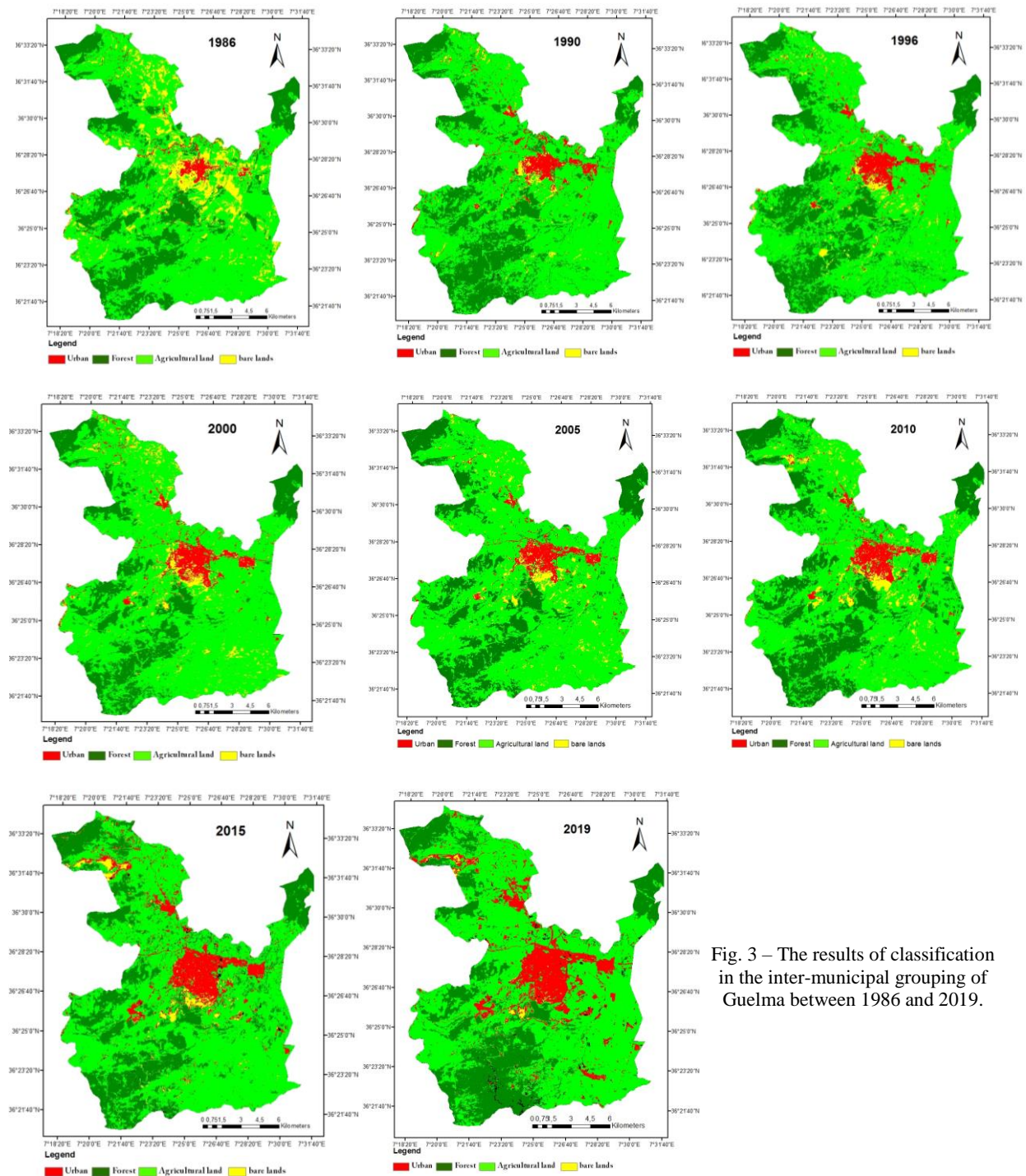


Fig. 3 – The results of classification in the inter-municipal grouping of Guelma between 1986 and 2019.

To further explain urbanization during the study period in Guelma's inter-municipal classification, the areas of different land cover and their changes were calculated, and are presented in Fig. 4.

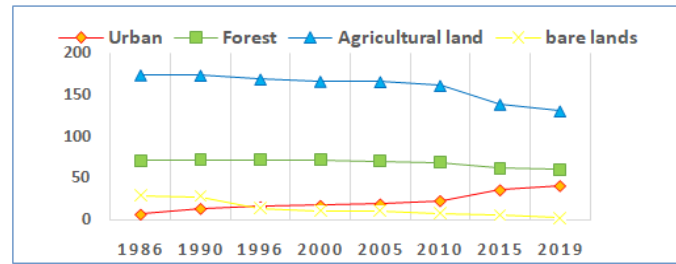
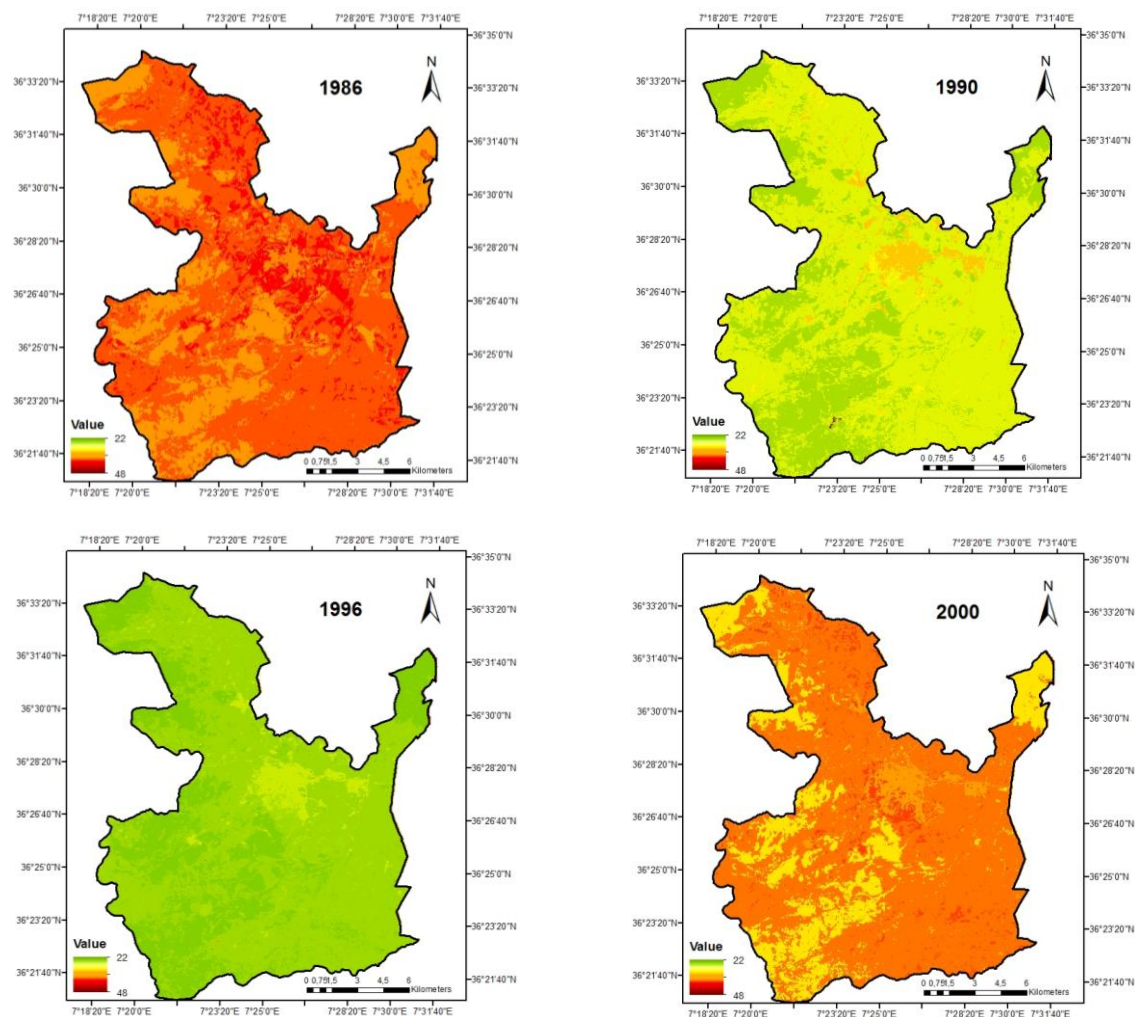


Fig. 4 – Urban land cover change in the inter-municipal grouping of Guelma from 1986 to 2019.

Fig. 4 reveals that there is a rising trend in the urban area from “6, 5 km²” to “40, 88 km²” in 1986 and 2019 respectively. However, the area of bare land, agriculture land and forest has decreased. For the bare land, the area decreases from 29.33 km² in 1986 to 1.98 km² in 2019. For the agricultural land, the surface has decreased from 173.22 ha in 1990 to 130.48 ha in 2019. For the forest, the area has decreased from 71.14 km² in 2005 to 60.34 km² in 2019. Based on these findings, it is concluded that the urban land cover increase is directly proportional to the reduction in green cover especially in the last period. The result of analysis is consistent with Guechi *et al.*, 2017.



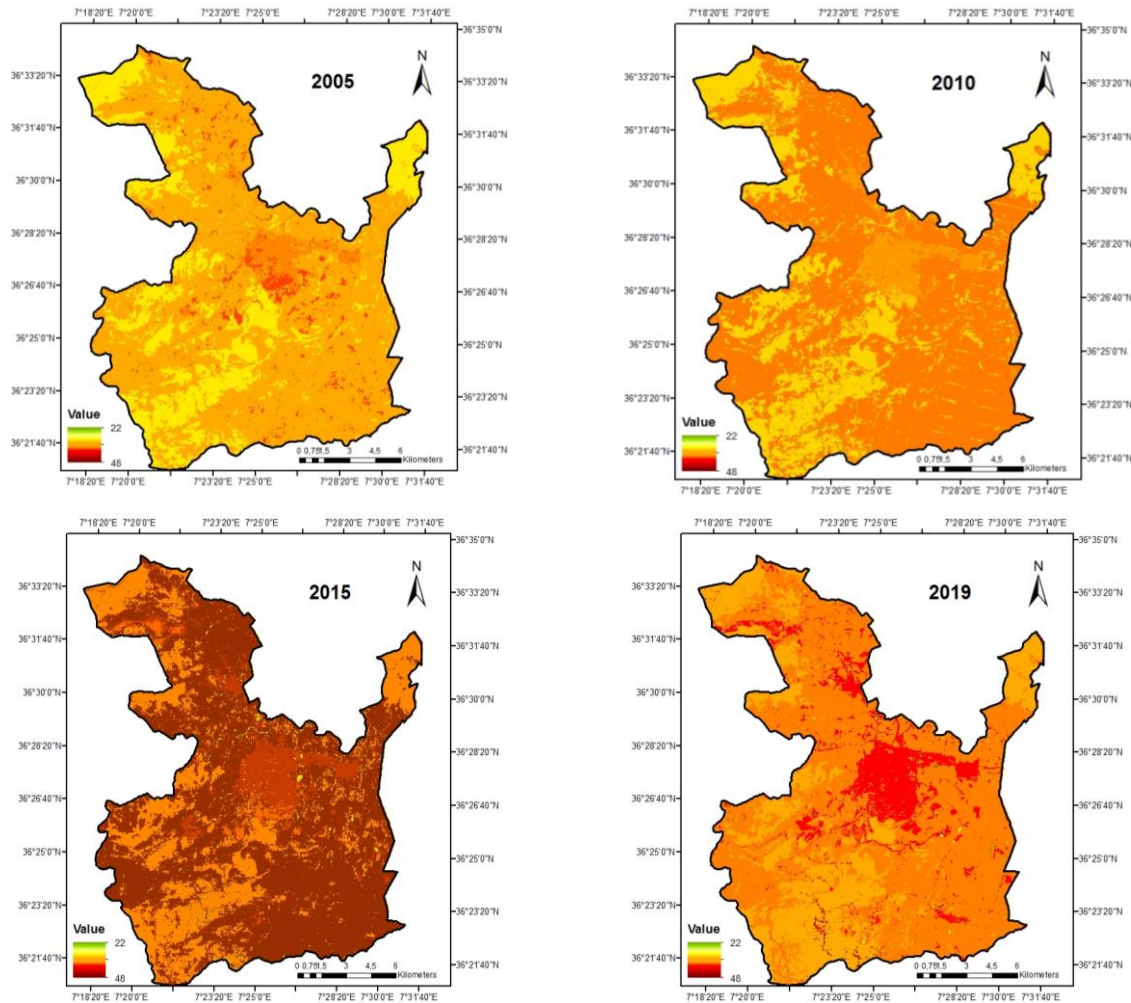


Fig. 5 – Mean land surface temperature in the inter-municipal grouping of Guelma for corresponding years to land cover classification.

The LSTs estimated from Landsat images are shown in Fig. 5 which reveals a clear gradient between urban areas, bare land, agriculture land and forests from 1986 to 2019. It illustrates the temperature increase in urban setting in the 1990 and 1996. This is principally owing to higher radiant temperatures in urban surface materials. The results of this analysis are consistent with other studies related to the rise in LST due to the changing of LULC (Carleton *et al.*, 2016; Tan *et al.*, 2020; Das *et al.*, 2020). However, for the years: 2000, 2005, 2010 and 2015, agricultural land had the highest temperature owing to the absence of vegetation. The mean temperature values of LST for each class are presented in Table 3.

Table 3

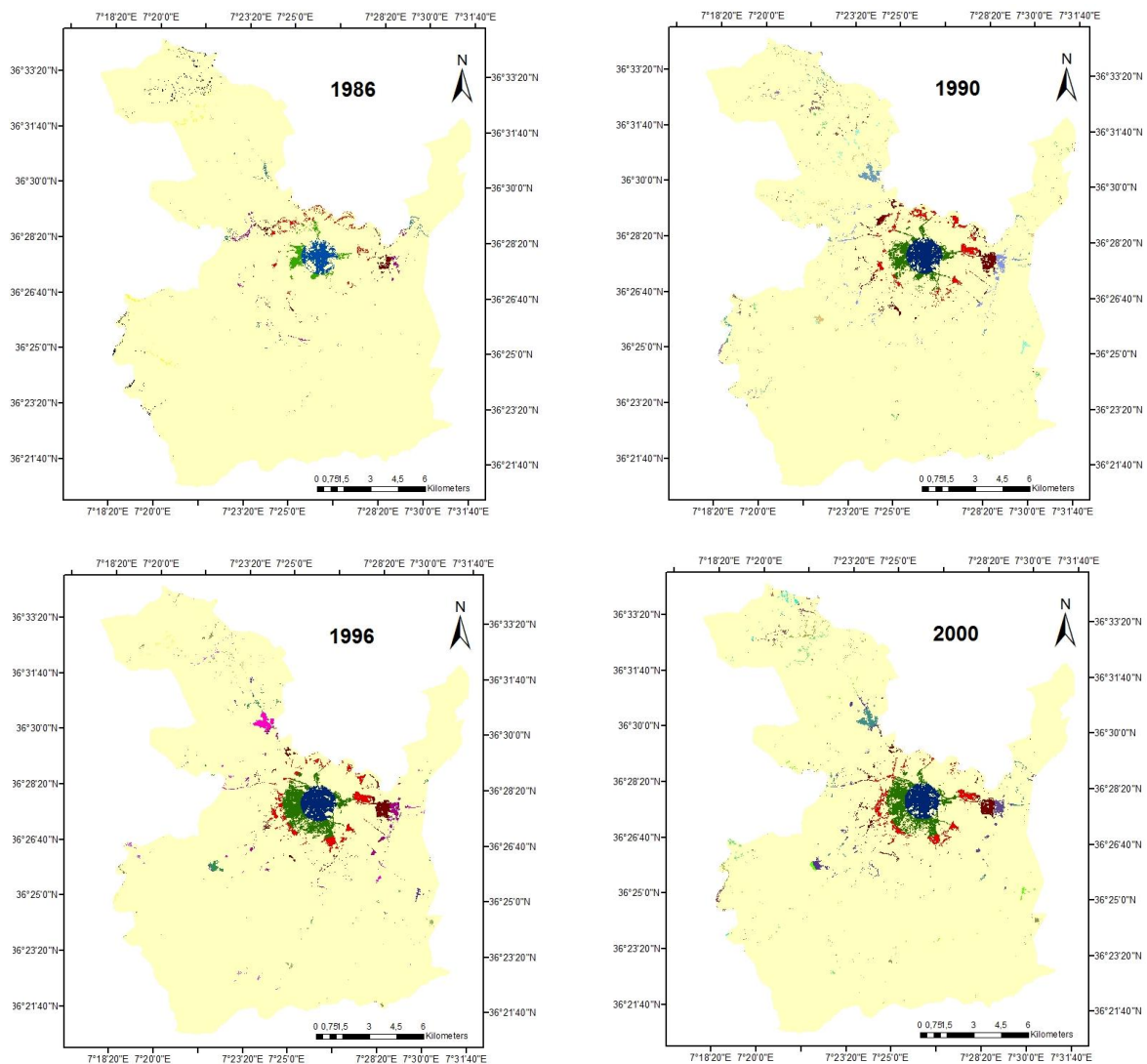
Mean LST (C°) for corresponding urban land cover

	1986	1990	1996	2000	2005	2010	2015	2019
Urban	38.25	31.43	27.24	35.61	37.17	33.33	47.05	41.90
Forest	37.12	26.55	22.51	31.17	33.90	27.46	44.02	37.78
Agricultural land	40.12	29.75	25.33	36.53	37.96	33.46	47.74	40.80
Bare lands	41.31	30.79	25.56	37.53	37.98	32.83	46.21	40.07

In 1986, the average temperature of urban settings was 38.27 C° , whereas, in 2019 it reached 41.90 C° . When the average temperature values for every class are calculated, the lowest temperature values were observed in forest bodies with 27.26 C° in 1986 and 37.78 C° in 2019. It is found to be the same result with Aboelnour and Engel, 2018; Pal and Ziaul, 2017.

4.3. Urban density and its relationship with LST

After classification, multi-buffer rings are created for every 1 km distance from 1 km to 16km from Guelma centre to outside.



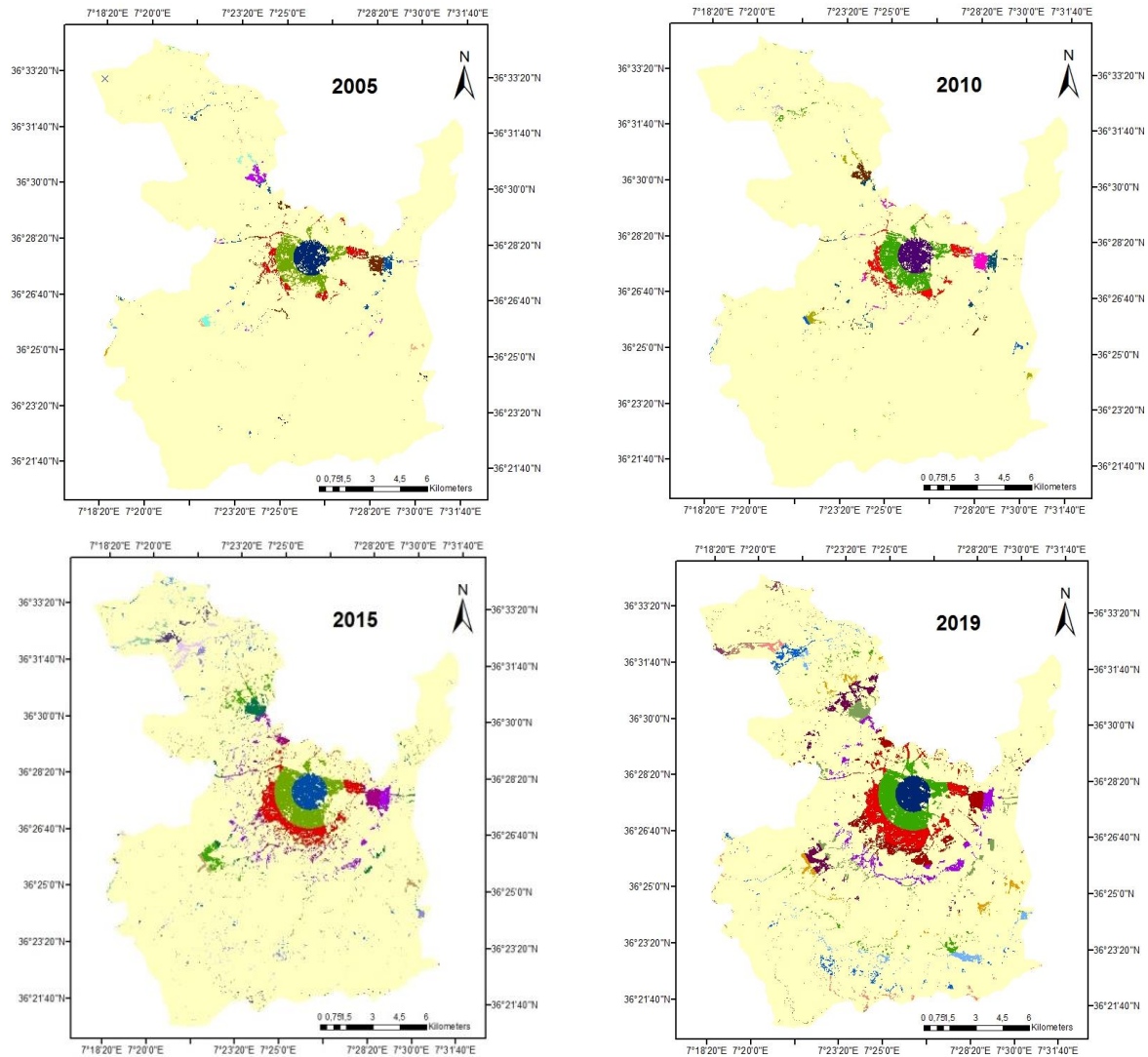


Fig. 6 – Multi-buffer ring analysis of the inter-municipal grouping of Guelma from 1986 to 2019.

The principle aim of applying the method of multi-buffer ring is to determine the spatial and temporal relationships (Fonseka *et al.*, 2019). Some attractive patterns in the urban land distribution throughout a variety of buffer zones can be observed in Fig. 6. The various zones or rings have embodied various densities. A pattern analysis was applied to obtain the relationship of urban density shift and mean LST in the inter-municipal grouping of Guelma. The findings are presented in Fig. 6.

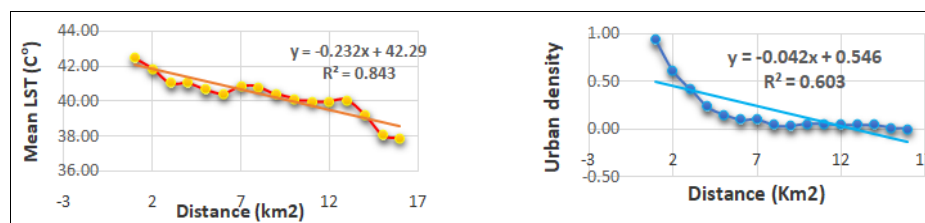


Fig. 7 – Trend analysis of average urban density, average temperature with distance from the city centre of Guelma.

As predicted, it is clear that in both diagrams the density in the inter-municipal grouping of Guelma in 2019 tends to decline outward from the centre. It is the same for the mean LST. However, it is difficult to validate the precise relationship between urban density and LST by in-situ measurements because emissivity can be affected by some factors, such as the composition of all land cover classes within each pixel which was also proven by past research (Fonseka *et al.*, 2019; Ahmad *et al.*, 2016).

4.4. Urban form and its relationship with LST

The form indices and mean LST are calculated and presented in Table 4. The indices' values equal to one express a compact form, whereas the indices close to zero imply an excessive sprawl (Guérois, 2003).

Table 4

Mean LST (C°) for corresponding urban form indices

	I1	I2	I3	I4	I5	I6	Mean LST	Min LST	Max LST
Guelma	0,3	0,61	0,58	0,44	0,34	0,18	41,76	38,82	49,74
Bel Khair	0,54	0,6	0,57	0,51	0,46	0,47	41,77	39,82	44,97
Ben Djarah	0,41	0,73	0,46	0,43	0,44	0,65	41,49	39,13	45,58
El Fjouj	0,22	0,36	0,35	0,27	0,21	0,42	42	40,4	44,01

According to Table 4, we can say that the city of El Fdjouje had a more spread out and warmer form. The urban form of Guelma and Belkhir is elongated and less compact with a medium temperature in contrast to that of the municipality of Bendjarah, which has a compact non-elongated shape and a lower temperature compared to the other municipalities. Therefore, we can say that the elongated urban form is warmer than the compact form.

4.5. Landscape patterns and its relationship with LST

Based on data of June 19th, 2019, the grid samples of LC and LST are presented in Fig. 8. The quantitative relation between LST and each LC's landscape pattern was studied and represented in Figs. 9, 10 and 11.

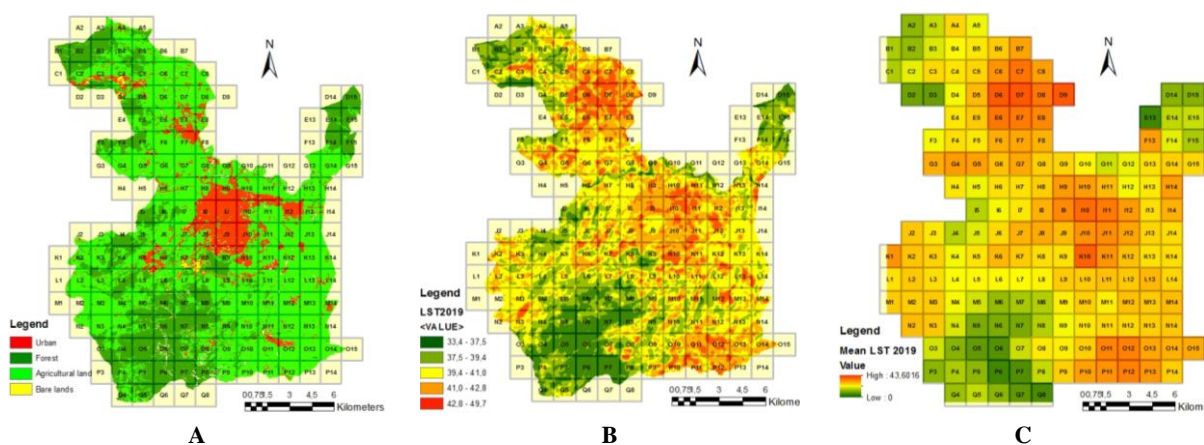


Fig. 8 – Sample grid in the study area. (A) Slice of LC figure, (B) Slice of LST figure and (C) Slice of mean LST figure.

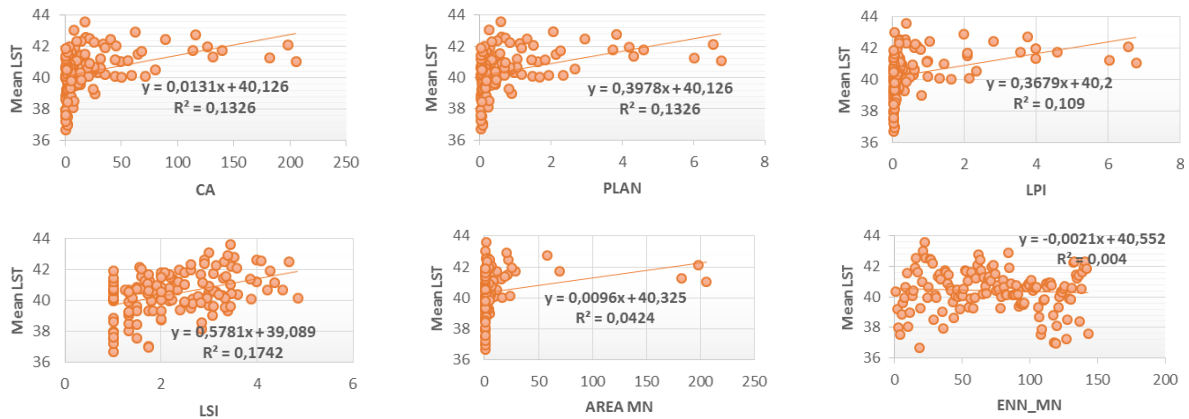


Fig. 9 – The relationship between urban Landscape Pattern Indices and LST.

For the urban space, Fig. 9 reveals that there is a positive relationship between the mean LST and CA $R = 0.36$, PLAN $R = 0.36$, LPI $R = 0.31$, LSI $R = 0.41$, AREA-MN $R = 0.20$ and a negative relationship with ENN-MN. Since CA is important, a large PLAND and LPI signifies a huge part of the area's urban and large patch size. Thus, the LST average is high. Having a large ENN MN indicated a fragmented and dispersed urban surface distribution. This indicates that the LST average is low. A large LSI signifies a complex form of the urban surface which leads to massive surface contact with the environment. Therefore, the average LST around it increases the same as the results with Hongyu *et al.*, 2019.

According to Fig. 10, we note that there is a negative relationship between the mean LST and CA $R = -0.67$, PLAN $R = -0.67$, LPI $R = -0.68$, LSI $R = -0.14$, AREA-MN $R = -0.64$ and a positive one with ENN-MN $R = 0.26$. High fragmentation signifies a mean dispersed GL distribution and long distances between patches. The complex shape of the forest area landscape, important CA, large PLAND and LPI, and large patch size which mean a huge part of land have low mean LST. The results are the same with Li *et al.*, 2013.

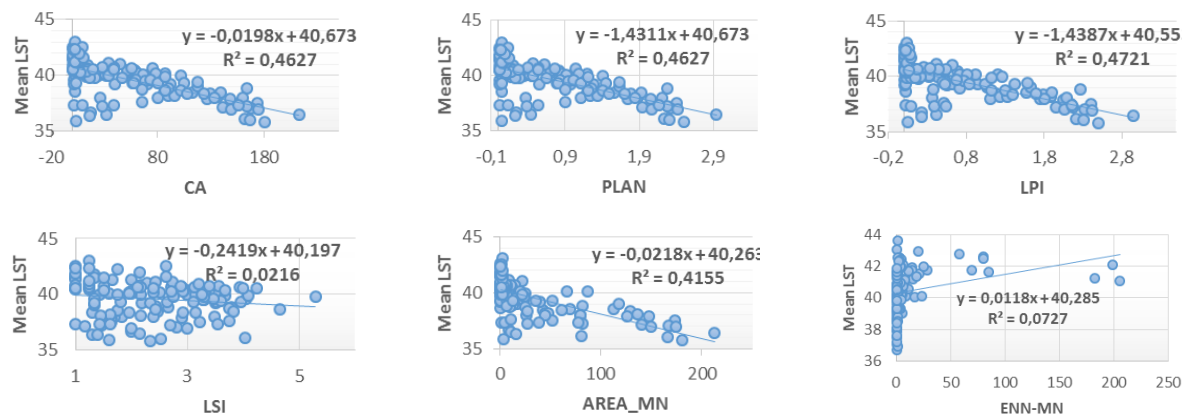


Fig. 10 – The relationship between forest Landscape Pattern Indices and LST.

According to Fig. 11, just as the urban space, the indices of the agricultural land (CA, PLAN, and LPI) display positive correlations with LST, except LSI, which displays a negative correlation. This contrasts what is reported in most previous studies (Li *et al.*, 2013; Hongyu *et al.*, 2019).

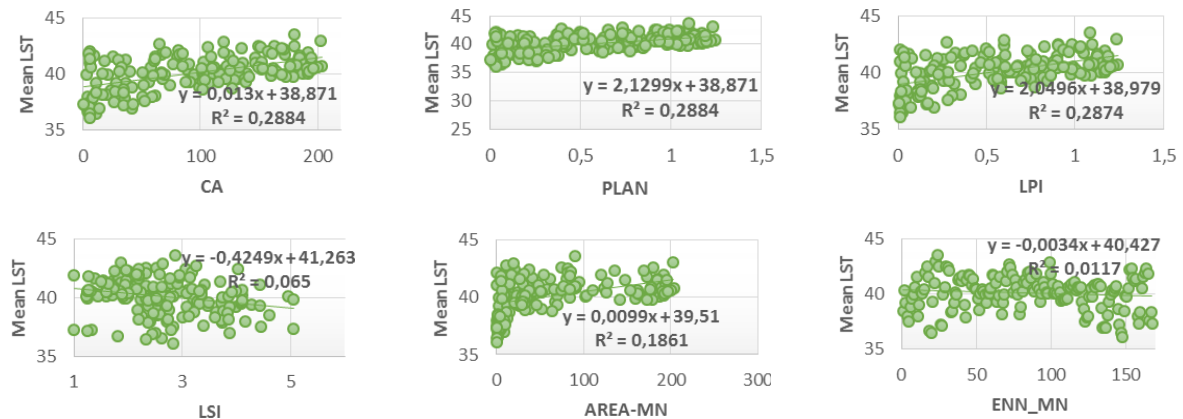


Fig. 11 – The relationship between agriculture Landscape Pattern Indices and LST.

4.6. Spatiotemporal Pattern of NDVI, NDBI Dynamics and Its Relationship with LST

In order to determine the relationship between NDBI, NDVI and LST, 168 sample points randomly collected from LST, NDBI and NDVI images were used to perform the appropriate regression. The coefficients of the Pearson correlation were calculated and presented in Table 5.

Table 5

LST- NDVI, LST-NDBI relationships from 1986 to 2019.

	1986	1990	1996	2000	2005	2010	2015	2019
NDVI, LST correlation coefficient	-0.68	-0.72	-0.74	-0.83	-0.78	-0.69	-0.68	-0.72
NDBI, LST correlation coefficient	0.47	0.65	0.66	0.60	0.50	0.40	0.52	0.50

The NDVI is negatively correlated with LST. Thus, the areas with the least vegetation are experiencing higher LST. On the other hand, the NDBI and the LST are positively correlated. The results are similar to those found by Naserikia *et al.*, 2019, Mathew, Khandelwal, &Kaul, 2018.

The average and weak correlation between LST and NDBI in 1986, 2000, 2005, 2010, 2015 and 2019 might be correlated with a higher LST. In order to determine the correlation between LST (dependent variable), NDBI and NDVI (independent variables), the multiple linear regressions were utilized. The data utilized in the regression model are represented in a graphic form with a 3D space in Fig. 12.

The LST range in the 3D scatterplot was presented in the form of balls which change in terms of size and colour according to the LST values of each year. The larger-sized balls had high LSTs, low vegetation, and high built-up features. However, the root with smaller balls displays a low LST, low built-up, but highly-vegetated pixels (Naserikia *et al.*, 2019). The red colours, which represent the hotter spots, increased particularly in 1986, 2000, 2005, 2010, 2015 and 2019. On this note, the ones in 2015 showed greater hotter spots than the ones from the other years. It was noticed that in 1990 and 1996, the number of balls which are characterized with reasonably fresh surface temperatures was significantly higher. The value of LST increases with the increasing surface brightness NDBI and reducing vegetation NDVI on the surface (1986, 2000, 2005, 2010 and 2015), and vice versa.

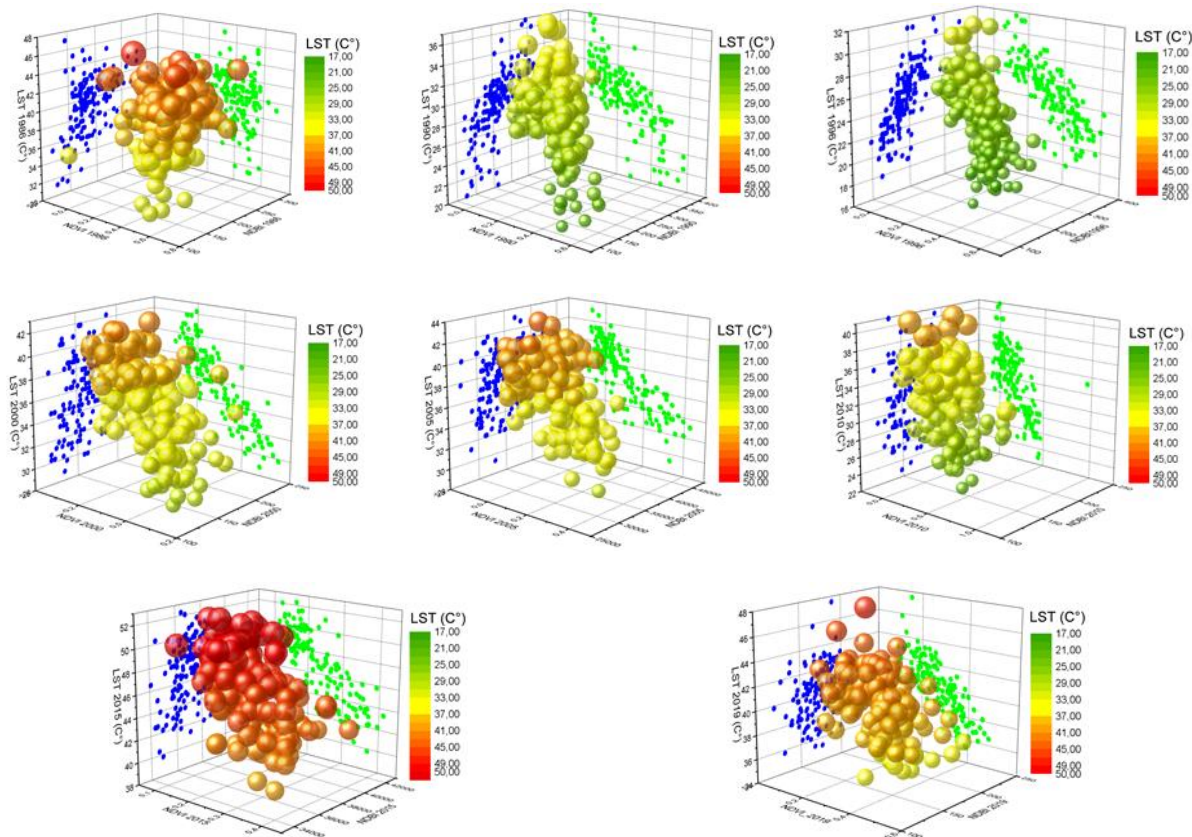


Fig. 12 – 3D scatterplots of the LST- NDVI and LST-NDBI relationships from 1986 to 2019.

5. DISCUSSIONS

5.1. Urban expansion: A mutation of LU / LC and its intensification on LST

Like all medium-sized cities in Algeria, Guelma is affected by rapid and massive urban growth which has strongly disrupted the space (Fig. 3, Fig. 4). Thus, profound spatial and environmental transformations are being generated. The position of Guelma in the centre places these communes in its attraction range (Guechi *et al.*, 2017; PDAU., 2013). Because of its environmental attraction, the city has undergone explosive impermeable growth in the form of residential, commercial, retail, transit networks, and parking lots. This growth was at the expense of transforming LU / LC classes such as urban, agriculture, forests and bare lands. This modification pattern in LU / LC dynamics has significantly altered the scenario of the LST distribution (Wang *et al.*, 2018; Gogoi *et al.*, 2019; Zhao *et al.*, 2013; Li *et al.*, 2018; Pal and Ziaul, 2017; Weng *et al.*, 2004).

Vegetation also displays lower temperatures compared to urban areas along the time scale. This can be best clarified by the fact that through the transpiration cycle, forest or vegetation can reduce the amount of heat contained in the soil or the soil surface. Compared to vegetation areas, higher temperature values are recorded in both urban and bare lands. These results were found to be in line with the actual studies (Fonseka *et al.*, 2019; Gong *et al.*, 2006). Urban areas experience higher temperatures principally owing to the construction materials used. One reason for having high temperature values for bare land is that the majority of bare fields are in areas where there is ongoing development and reduction in vegetation cover (Fonseka *et al.*, 2019).

As presented in Fig. 5 and Table 3, agricultural land has the highest temperature in the years of 2000, 2005, 2010 and 2015 owing to the absence of vegetation. The period of last June in Guelma is known as the time of barley and wheat harvest. However, on 19/06/2019, the LST of the urban space displayed the most important value compared to the LST of the agricultural land, the forest and the bare land, although the agricultural land displays land without vegetation. These results confirm that the strong urbanization which marked the past years has exerted an influence on the increase of LST. (Das *et al.*, 2020; Zhao *et al.*, 2013; Li *et al.*, 2018). There is a possible rise in LST over time due to the substitution of green cover by urban soil areas. Generally, there was a noticeable increase in the mean LST of 3.65 °C for urban areas. In this research, the majority of the urban expansion resulted from the conversion of the green cover. The problem in this case study is that the future urbanization of the municipality of Guelma will be directed towards the neighbouring municipalities (the revision of the PDAU 2013) which are surrounded by land with high agricultural potential (Fig. 4). It is well known that the gradual replacement of natural surfaces by constructed surfaces, through urbanization, is the main reason of the LST increase.

5.2. Landscape characteristic effect on LST

In this analysis, the temperature variation and standard deviation show that there are significant differences in a particular form of land-cover as well as the similarities between various types of land-covers. More studies that are recent have shown similar findings (Gogoi *et al.*, 2019; Das *et al.*, 2020).

In this research, the broad region, the low degree of fragmentation of the landscape, and complex outlines have led to reduced forest LST values and increased urban LST values (Fig. 9, Fig. 10). However, like the urban space, the indices of the agricultural land (CA, PLAN, and LPI) display positive correlations with LST, while LSI displays a negative correlation (Fig. 11). These results are explained by the absence of the green cover in most of the agricultural land because of the harvest. Thus, the bare ground reflects an important quantity of the temperature. For LSI, the complex composition of spaces where this displays vegetation is explained by the deprivation of the LST valuations. Our findings are consistent with several other studies reported in literature in other regions. Estoque *et al.* 2017 has found that the difference between the mean LST of built-up land and vegetation cover was 2.7°C in 1987 and 3.4°C in 2015. However, Boyan *et al.*, 2018 have found a gap of 1.3°C.

Therefore, NDVI and NDBI are not sufficient indices for the analysis of LST in towns dominated by barren land which absorbs a significant volume of solar radiation. Mathew *et al.*, 2018 have also demonstrated the ineffectiveness of NDBI in Surface LST Intensity studies, because bare soils and dry vegetation covers show a high spectral reflection in the SWIR band, resulting in positive NDBI values for drier plants and low NDBI values for barren soil compared to built-up areas. It is the same for GUELMA, especially in the summer. A negative relationship was found between vegetation indices and LST (Table 5), which was most likely owing to the impact of surface thermal inertia and evapotranspiration. Moreover, the relationship between the LST variations and NDVI variations is supposed to be direct.

6. CONCLUSIONS

Multidisciplinary theories and methods were used in this research to analyse the effect of LULC characteristics on the LST. The results show that in the inter-communal grouping of Guelma the LULC type has changed significantly. The urban/built-up areas of Guelma city have dramatically expanded, whereas the green cover has declined. These results indicate that the changes in the area's LULC type are related to the rapid and massive urban growth. The LSTs of different LCs are significantly different. Changes to LULC have been followed by changes to the LST. In the 1990s, 1996 having much green cover, the temperature of the urban setting was the most important, while the

years 1986, 2000, 2005, 2010 and 2015, which witnessed the reduction of vegetation, agricultural land, bare land and built-up areas had almost the same temperature. This confirms the role of vegetation in decreasing LST. Moreover, the variation in temperature between the urban setting and forest areas has significantly widened. Therefore, the excessive presence of vegetation was a crucial factor that influences LST. Landscape level indices are used to define the overall LC status characteristics, whereas patch type indices concentrate on the LCT types' morphology and structure. The selected landscape indices include total area (CA), percent landscape (PLAN), largest patch index (LPI), mean patch area (AREA_MN), landscape shape index (LSI), and the Euclidean nearest neighbour distance (ENN). These are typical and frequently used hints in landscape research. For the urban space, we note that there is a positive relationship between the mean LST and CA, PLAN, LPI, LSI, AREAMN, and a negative relationship with ENN-MN, and vice versa for forest area. Broad regions, a low landscape fragmentation degree and complex outlines have reduced forest LST values and increased urban LST values. In comparison to the LST of the sprawl form, the LST of the compact form is low. The results of the LST/NDVI and LST/NDBI relationship have shown a negative correlation and positive relationship, respectively. In the context of LST /NDVI, it can be said that a higher NDVI led to a lower LST and vice versa for the relation between LST/NDBI, where the depletion of green cover had a significant role in the escalation of LST, since vegetation can lower temperatures.

Overall, findings have proved the ability of Landsat multi-temporal images that can precisely measure the trend of transition in LULC and LST in Guelma. Furthermore, the combination of RS and GIS may offer a beneficial tool for surveying, tracking the landscape and the extent of land-cover shifts. Consequently, the knowledge obtained from the outputs of change identification will help to explain the complexities of LULC transition to help policymakers anticipate and schedule future changes in Guelma, achieve long-term stabilization of soil and water supplies and their effects on climate change, and thereby define the evolution of urban building lands.

REFERENCES

- Aboelnour M, Engel, BA (2018), *Application of remote sensing techniques and geographic information systems to analyse land surface temperature in response to land use/land cover change in Greater Cairo Region, Egypt*. Journal of Geographic Information System **10**(01): 57.
- Ahmad, F., & Goparaju, L. (2016), *Analysis of urban sprawl dynamics using geospatial technology in Ranchi City, Jharkhand, India*. Journal of Environmental Geography, **9**(1–2), pp. 7–13.
- Aouissi, A. (2010.), *Microbiologie et physico-chimie de l'eau des puits et des sources de la région de Guelma (Nord-est de l'Algérie)*. Thèse de Magistère, Université 8 Mai 1945. Guelma, Algerie.
- Asgarian, A., Amiri, B. J., & Sakieh, Y. (2015), *Assessing the effect of green cover spatial patterns on urban land surface temperature using landscape metrics approach*. Urban Ecosystems, **18**(1), pp. 209–222.
- Benenson, W., Harris, J., Stöcker, H., & Lutz, H. (2002), *Handbook of Physics*. New York, NY, USA: Springer.
- Boogaard, F., Vojinovic, Z., Chen, Y. C., Kluck, J., & Lin, T. P. (2017), *High resolution decision maps for urban planning: A combined analysis of urban flooding and thermal stress potential in Asia and Europe*. In MATEC Web of Conferences (Vol. **103**, pp. 04012). EDP Sciences.
- Boori, M. S., Netzband, M., Choudhary, K., & Voženílek, V. (2015), *Monitoring and modeling of urban sprawl through remote sensing and GIS in Kuala Lumpur, Malaysia*. Ecological Processes, **4**(1), 15.
- Brown, D. R. N., Jorgenson, M. T., Kielland, K., Verbyla, D. L., Prakash, A., & Koch, J. C. (2016), *Landscape effects of wildfire on permafrost distribution in interior Alaska derived from remote sensing*. Remote Sensing, **8**(8).
- Carleton, T., & Hsiang, S. (2016), *Social and economic impacts of climate*. Science.
- Chander, G., & Markham, B. (2003), *Revised Landsat-5 TM radiometric calibration procedures and post-calibration dynamic ranges*. IEEE Transactions on Geoscience and Remote Sensing, **41** (11), pp. 2674–2677.
- Chander, G., Markham, B., & Helder, D. (2009), *Summary of current radiometric calibration coefficients for Landsat MSS, TM, ETM+, and EO-1 ALI sensors*. Remote Sensing of Environment, **113**(5), pp. 893–903.
- Chen, Y., & Yu, S. (2017), *Impacts of urban landscape patterns on urban thermal variations in Guangzhou, China*. International journal of applied earth observation and geoinformation, **54**, pp. 65–71.
- Das, N., Mondal, P., Sutradhar, S., & Ghosh, R. (2020), *Assessment of variation of land use/land cover and its impact on land surface temperature of Asansol subdivision*. The Egyptian Journal of Remote Sensing and Space Science.
- Estoque, R. C., & Murayama, Y. (2017), *Monitoring surface urban heat island formation in a tropical mountain city using Landsat data (1987–2015)*. ISPRS Journal of Photogrammetry and Remote Sensing, **133**, pp. 18–29.

- Estoque, R., Murayama, Y., & Myint, S. (2017), *Effects of landscape composition and pattern on land surface temperature: An urban heat island study in the megacities of Southeast Asia*. *Sci. Total Environ*, 577.
- Ferrelli, F., Huamantincio Cisneros, M.A., Delgado, A.L., & Piccolo, M.C. (2018), *Spatial and temporal analysis of the LST-NDVI relationship for the study of land cover changes and their contribution to urban planning in Monte Hermoso, Argentina*.
- Fonseka, H., Zhang, H., Sun, Y., Su, H., & Lin, H. L. (2019), *Urbanization and Its Impacts on Land Surface Temperature in Colombo Metropolitan Area, Sri Lanka, from 1988 to 2016*. Remote sensing.
- Gogoi, P.P., Vinoj, V., Swain, D., Roberts, G., Dash, J., & Tripathy, S. (2019), *Land use and land cover change effect on surface temperature over Eastern India*. *Scientific reports*, 9(1), pp. 1–10.
- Gong, A., Chen, Y., Li, J., Gong, H., & Li, X. (s.d.). (2006), *Spatial distribution patterns of the urban heat island based on remote sensing images: A case study in Beijing, China*. In *Proceedings of the 2006 IEEE International Geoscience Remote Sensing Symposium*.
- Green, K., Kempka, D., & Lackey, L. (1994), *Using remote sensing to detect and monitor land-cover and land-use change*. *Photogrammetric Engineering & Remote Sensing*, 60, pp. 331–337.
- Guechi I., Alkama Dj . (2017), *Apport de la télédétection pour la cartographie diachronique de l'étalement urbain et l'analyse morphologique de l'agglomération de Guelma*. *Courrier du Savoir – N°24*, pp.73–80.
- Guha, S., Govil, H., Dey, A., & Gill, N. (2018), *Analytical study of land surface temperature with NDVI and NDBI using Landsat 8 OLI and TIRS data in Florence and Naples city, Italy*. *European Journal of Remote Sensing*, 51(1), 667–678.
- Hongyu, D., Jinquan, A., Yongli, C., & Liu, H. J. (2019), *Combined Effects of the Surface Urban Heat Island with Landscape Composition and Configuration Based on Remote Sensing: A Case Study of Shanghai, China*. *Sustainability*.
- Imhoff, M., Zhang, P., Wolfe, R., & Bounoua, L. (2010), *Remote sensing of the urban heat island effect across biomes in the continental USA*. *Remote Sens. Environ*, 114 (3), pp. 504–513.
- Inc, E. (1999), *Erdas Field Guide*. Erdas Inc. Atlanta, Georgia.
- Jain, M., Dimri, A. P., & Niyogi, D. (2017), *Land-Air Interactions over Urban-Rural Transects Using Satellite Observations: Analysis over Delhi, India from 1991–2016*. *Remote Sensing*, 9(12), 1283.
- Jensen, J. (1995), *Introductory Digital Image Processing a Remote Sensing Perspective* (éd. Second Edition). New Jersey, Englewood Cliffs: Prentice-Hall.
- Junxiang, L., Conghe, S., Lu, C., Feige, Z., Xianlei, M., & Jianguo, W. (2011), *Impacts of landscape structure on surface urban heat islands: a case study of Shanghai, China*. *Remote Sens. Environ*, 115, pp. 3249–3263.
- Kam, T. (1995), *Integrating GIS and remote sensing techniques for urban land-cover and land-use analysis*. *Geocarto International*, 10, pp. 39–49.
- Killian, J. (2014), *Magnet-Cities*. Available online: <https://home.kpmg.com/uk/en/home/insights/2014/07/magnetcities.html>.
- Kimuku, C.W. and Ngigi, M. (2017), *Study of Urban Heat Island Trends to Aid in Urban Planning in Nakuru County-Kenya*. *Journal of Geographic Information System*, 9, pp. 309–325.
- Kong, F., Yin, H., James, P., Hutyra, L., & He, H. (2014), *Effects of spatial pattern of greenspace on urban cooling in a large metropolitan area of eastern China*. *Landsc. Urban Plan*, 128, pp. 35–47.
- Kumar, K., Bhaskar, P., & Padmakumari, K. (2012). *Estimation of land surface temperature to study urban heat island effect using LANDSAT ETM+ image*. *Int. J. Eng. Sci. Technol*, 4 (2), pp. 771–778.
- Landsat, N. (s.d.), *Science Data Users Handbook*. 2011–03–11. Consulté le October 23, 2019, sur http://landsathandbook.gsfc.nasa.gov/inst_cal/prog_sect8_2.html.
- Landsat, N. (s.d.), *Science Data Users Handbook*. 2015-june. <http://landsat.usgs.gov/18handbook.php>. Accessed 30 September 2019.
- Li, B., Wang, W., Bai, L., Wang, W., & Chen, N. (2018), *Effects of spatio-temporal landscape patterns on land surface temperature: a case study of Xi'an city, China*. *Environmental Monitoring and Assessment*, 190(7), 419.
- Li, X., Zhou, W., & Ouyang, Z. (2013), *Relationship between land surface temperature and spatial pattern of greenspace: What are the effects of spatial resolution?* *Landsc. Urban Plan*, 114, pp. 1–8.
- Liu, S., Su, H., Zhang, R., Tian, J., & Wang, W. (2016), *Estimating the surface air temperature by model*. *Advances in Meteorology*.
- Lo, C., Quattrochi, D., & Luvall, J. (1997). *Application of high-resolution thermal infrared remote sensing and GIS to assess the urban heat island effect*. *Int. J. Remote Sens*, 18, pp. 287–304.
- Loveland, T., Sohl, S., Stehman, A., Gallant, K., & Saylor, N. D. (2002), *A strategy for estimating the rates of recent United States land-cover changes*, *Photogrammetric Engineering & Remote Sensing*, 68(10), pp. 1091–1099.
- Maimaitiyiming, M., Ghulam, A., Tiyip, T., Pla, F., Latorre-Carmona, P., Halik, Ü., Caetano, M. (2014), *Effects of green space spatial pattern on land surface temperature: Implications for sustainable urban planning and climate change adaptation*. *ISPRS J. Photogramm. Remote Sens*, 89, pp. 59–66.
- Martinelli, L., & Matzarakis, A. (2017), *Influence of height/width proportions on the thermal comfort of courtyard typology for Italian climate zones*. *Sustainable Cities and Society*, 29, pp. 97–106.
- Mathew, A., Khandelwal, S., & Kaul, N. (2018), *Spatio-temporal variations of surface temperatures of Ahmedabad city and its relationship with vegetation and urbanization parameters as indicators of surface temperatures*. *Remote Sens. Appl. Soc. Environ*.
- Meineke, E., Dunn, R., & Frank, S. (2014), *Early pest development and loss of biological control are associated with urban warming*. *Biol. Lett*.
- Mitchell, B. C. (2011). *Urbanization and Land Surface Temperature in Pinellas County, Florida, Graduate Theses and Dissertations*. Récupéré sur <http://scholarcommons.usf.edu/etd/3250>.

- Myint, S., Wentz, E., Brazel, A., & Quattrochi, D. (2013), *The impact of distinct anthropogenic and vegetation features on urban warming*. *Landscape Ecol*, **28** (5), pp. 959–978.
- Naserikia, M., Asadi Shamsabadi, E., Rafieian, M., & Leal Filho, W. (2019), *The urban heat island in an urban context: A case study of Mashhad, Iran*. *International Journal of Environmental Research and Public Health*, **16**(3), 313.
- Pal, S., & Ziaul, S. (2017), *Detection of land use and land cover change and land surface temperature in English Bazar urban centre*. *Egyptian Journal of Remote Sensing and Space Science*, **20**(1), pp. 125–145.
- Pal, S., & Ziaul, S.K. (2017), *Detection of land use and land cover change and land surface temperature in English Bazar urban centre*. *The Egyptian Journal of Remote Sensing and Space Science*, **20**(1), pp. 125–145.
- Peng, J., Xie, P., Liu, Y., & Ma, J. (2016), *Urban thermal environment dynamics and associated landscape pattern factors: A case study in the Beijing metropolitan region*. *Remote Sens. Environ*, **173**, pp. 145–155.
- Plocoste, T., Jacoby-Koaly, S., Molinić, J., & Petit, R. (2014), *Evidence of the effect of an urban heat island on air quality near a landfill*. *Urban Clim*, **10**, pp. 745–757.
- Pushpendra, S., Singh, Vivekanand.T, & Anil.K. (2014), *Analysis of Supervised Maximum Likelihood Classification for Remote Sensing Image*, IEEE International Conference on Recent Advances and Innovations in Engineering (ICRAIE – 2014). Jaipur, India.
- Quattrochi, D., & Luval, J. (1999), *Thermal infrared remote sensing for analysis of landscape ecological processes: methods and applications*. *Landscape Ecol*, **14** (6), pp. 577–598.
- Radhi, H., Fikry, F., & Sharples, S. (2013), *Impacts of urbanisation on the thermal behaviour of new built up environments: a scoping study of the urban heat island in Bahrain*. *Landscape Urban Planning*, **113**, pp. 47–61.
- Rahman, M. (2016), *Detection of land use/land cover changes and urban sprawl in Al-Khobar, Saudi Arabia: An analysis of multi-temporal remote sensing data*. *Int. J. Geo Inf*.
- Ridd, M., & Liu, J. (1998), *A comparison of four algorithms for change detection in an urban environment*. *Remote Sensing of Environment*, **63**, pp. 95–100.
- Rizwan, A., Dennis, L., & Chunho, L. (2008), *A review on the generation, determination and mitigation of Urban Heat Island*. *J. Environ. Sci.*, **20** (1), pp. 120–128.
- Santos, R. G., Prata-Shimomura, A. R., Correia, E., Franco, M. D. A. R., & Lopes, A. S. (2017), *Morfologia Urbana e Corredores de Ventilação como subsídio à Resiliência Urbana*. *Revista LABVERDE*, **8**(2), pp. 12–37.
- Singh, A. (1989), *Digital change detection techniques using remotely-sensed data*. *International Journal of Remote Sensing*, **10**, pp. 989–1003.
- Sohl, T. (1999), *Change analysis in the United Arab Emirates: An investigation of techniques*. *Photogrammetric Engineering & Remote Sensing*, **65**(4), pp. 475–484.
- Spence, M., Annez, P., & Buckley, R. (2009), *Urbanization and Growth*. Washington, DC, USA: Word Bank.
- Sun, H., Forsythe, W., & Waters, N. (2007), *Modeling urban land use change and urban sprawl*: Calgary, Alberta, Canada. *Netw. Spat. Econ*, **7**.
- Tan, J., Yu, D., Li, Q., Tan, X., & Zhou, W. (2020), *Spatial relationship between land-use/land-cover change and land surface temperature in the Dongting Lake area, China*. *Scientific Reports*, **10**(1), pp. 1–9.
- UNFPA. (Retrieved February 12, 2017, from <http://www.unfpa.org/urbanization>). Urbanization.
- USGS. (2014), *Using the USGS Landsat 8 product*. Retrieved December 11, 2014 from <https://landsat.usgs.gov/using-usgs-landsat-8-product>.
- Voogt, J., & Oke, T. (2003), *Remote sensing of urban climates*. *Remote Sensing of Environment*, **3**(86), pp. 70–84.
- Wang, R., Derdouri, A., & Murayama, Y. (2018), *Spatiotemporal simulation of future land use/cover change scenarios in the Tokyo metropolitan area*. *Sustainability*, **10**(6), 2056.
- Wang, Y. C., Hu, B. K., Myint, S. W., Feng, C. C., Chow, W. T., & Passy, P. F. (2018), *Patterns of land change and their potential impacts on land surface temperature change in Yangon, Myanmar*. *Science of the Total Environment*, **643**, pp. 738–750.
- Weng, Q. (2009), *Thermal infrared remote sensing for urban climate and environmental studies: methods, applications, and trends*. *ISPRS J. Photogrammetry Remote Sens*, **64** (4), pp. 335–344.
- Yang, F., & Chen, L. (2016), *Developing a thermal atlas for climate-responsive urban design based on empirical modeling and urban morphological analysis*. *Energy and Buildings*, **111**, pp. 120–130.
- Yang, X., & Lo, C. (2002), *Using a time series of satellite imagery to detect land use and land cover changes in Atlanta, Georgia metropolitan area*. *International Journal of Remote Sensing*, **9**, pp. 1775–1798.
- Yuan, F., & Bauer, M. (2007), *Comparison of impervious surface area and normalized difference vegetation index as indicators of surface urban heat island effects in Landsat imagery*. *Remote Sens. Environ*, **106** (3), pp. 375–386.
- Yuan, F., Sawaya, K. E., Loeffelholz, B. C., & Bauer, M. E. (2005), *Land cover mapping and change analysis in the Twin Cities Metropolitan Area with Landsat remote sensing*. *Remote Sensing of Environment*, **98**(2.3), pp. 317–328.
- Zhou, W., Huang, G., & Cadenasso, M. (2011), *Does spatial configuration matter? Understanding the effects of land cover pattern on land surface temperature in urban landscapes*. *Landsc. Urban Plan*, **102**, pp. 54–63.
- Zhou, W., Qian, Y., Li, X., Li, W., & Han, L. (2014), *Relationships between land cover and the surface urban heat island: seasonal variability and effects of spatial and thematic resolution of land cover data on predicting land surface temperatures*. *Landscape Ecol*, **29** (1), pp. 153–167.